Are Early Triassic extinction events associated with mercury anomalies? A reassessment of the Smithian/Spathian boundary extinction

Hammer, Øyvind ; Jones, Morgan T ; Schneebeli-Hermann, Elke ; Hansen, Bitten Bolvig ; Bucher, Hugo

Abstract: High concentrations of mercury, possibly connected with widespread volcanism of the Siberian Traps, have previously been associated with the Smithian/Spathian (Early Triassic) boundary (SSB) in the Sverdrup Basin, Tethyan sections in India and China, as well as with a shallow-water record in western Spitsbergen. We confirm this Hg/TOC anomaly in the deeper water record at Wallenbergfjellet, central Spitsbergen. However, both paleontological age control and carbon isotopes indicate that the Hg anomaly occurred mainly within strata of middle Smithian age. Therefore, this Hg anomaly is unlikely to be directly and causally related to mechanisms contributing to the late Smithian global extinction of nektonic faunas. The TOC and trace element data suggest generally more oxygenated conditions during the Smithian compared to the Spathian, which is at odds with the hypothesis that oxygen depletion may have been a global kill mechanism for the SSB extinction. Further work is needed to assess if precise timing and paleogeographic distribution of anoxia shows any consistent pattern or not during the Smithian and Spathian. The very abrupt lower limb of the positive carbon isotope excursion (CIE) and the coarser grain size immediately below the boundary between the Lusitaniadalen Member and the Vendomdalen Member indicate a substantial stratigraphic gap of latest Smithian age, a previously neglected signal shared with many other boreal SSB sections. Ammonoid age control also indicates that the onset of the late Smithian gap in the high latitudes was earlier than in the Tropics. The gradual end of the positive CIE contrasts with the frequent spike shape observed in tropical shelf records and is definitively earliest Spathian in age. The middle Smithian Hg anomaly in the Boreal record is only visible in the Hg/TOC values, and is associated with a possible shift in organic matter type from terrestrial to marine in the case of Spitsbergen. This suggests that the middle Smithian Hg/TOC anomaly in Spitsbergen may not unequivocally originate from volcanism, and calls for additional caution before interpreting Hg spikes as a volcanic proxy.

DOI: https://doi.org/10.1016/j.earscirev.2019.04.016

Hammer, Øyvind; Jones, Morgan T; Schneebeli-Hermann, Elke; Hansen, Bitten Bolvig; Bucher, Hugo (2019). Are Early Triassic extinction events associated with mercury anomalies? A reassessment of the Smithian/Spathian boundary extinction. Earth-Science Reviews, 195:179-190.
DOI: https://doi.org/10.1016/j.earscirev.2019.04.016

Accepted Manuscript

Are Early Triassic extinction events associated with mercury anomalies? A reassessment of the Smithian/Spathian boundary extinction

Øyvind Hammer, Morgan T. Jones, Elke Schneebeli-Hermann, Bitten Bolvig Hansen, Hugo Bucher

PII: S0012-8252(19)30167-9
DOI: https://doi.org/10.1016/j.earscirev.2019.04.016
Reference: EARTH 2844

To appear in: *Earth-Science Reviews*

Received date: 7 March 2019
Revised date: 10 April 2019
Accepted date: 11 April 2019

Please cite this article as: Ø. Hammer, M.T. Jones, E. Schneebeli-Hermann, et al., Are Early Triassic extinction events associated with mercury anomalies? A reassessment of the Smithian/Spathian boundary extinction, Earth-Science Reviews, https://doi.org/10.1016/j.earscirev.2019.04.016

Are Early Triassic extinction events associated with mercury anomalies? A reassessment of the Smithian/Spathian boundary extinction

Øyvind Hammer[1,*] ohammer@nhm.uio.no, Morgan T. Jones[2], Elke Schneebeli-Hermann[3], Bitten Bolvig Hansen[1], Hugo Bucher[3]

[1]Natural History Museum, University of Oslo, Pb. 1172 Blindern, 0318 Oslo, Norway

[2]Centre for Earth Evolution and Dynamics (CEED), Pb. 1028 Blindern, 0315 Oslo, Norway

[3]Paläontologisches Institut und Museum, Universität Zürich, Karl-Schmid-Strasse 4, 8006 Zürich, Switzerland

[*]Corresponding author.

Abstract

High concentrations of mercury, possibly connected with widespread volcanism of the Siberian Traps, have previously been associated with the Smithian/Spathian (Early Triassic) boundary (SSB) in the Sverdrup Basin, Tethyan sections in India and China, as well as with a shallow-water record in western Spitsbergen. We confirm this Hg/TOC anomaly in the deeper water record at Wallenbergfjellet, central Spitsbergen. However, both paleontological age control and carbon isotopes indicate that the Hg anomaly occurred mainly within strata of middle Smithian age. Therefore, this Hg anomaly is unlikely to be directly causally related to mechanisms contributing to the late Smithian global extinction of nektonic faunas. The TOC and trace element data suggest generally more oxygenated conditions during the Smithian compared to the Spathian, which is at odds with the hypothesis that oxygen depletion may have been a global kill mechanism for the SSB extinction. Further work is needed to assess if precise timing and paleogeographic distribution of anoxia shows any consistent pattern or not during the Smithian and Spathian. The very abrupt lower limb of the positive carbon isotope excursion (CIE) and the coarser grain size immediately below the boundary between the Lusitaniadalen Member and the Vendomdalen Member indicate a substantial stratigraphic gap of latest Smithian age, a previously neglected signal shared with many other boreal SSB sections. Ammonoid age control also indicates that the onset of the late Smithian gap in the high latitudes was earlier than in the Tropics. The gradual end of the positive CIE contrasts with the frequent spike shape observed in tropical shelf records and is definitively earliest Spathian in age. The middle Smithian Hg anomaly in the Boreal record is only visible in the Hg/TOC values, and is associated with a possible shift in organic matter type from terrestrial to marine in the case of Spitsbergen. This suggests that the middle Smithian Hg/TOC anomaly in Spitsbergen may not unequivocally originate from volcanism, and calls for additional caution before interpreting Hg spikes as a volcanic proxy.

Keywords: Earth crises; volcanism; extinction; carbon isotopes; Spitsbergen

1. Introduction

The Early Triassic is a fascinating epoch in Earth history, as ecosystems rebuilt and reformed in the aftermath of the end-Permian extinction event, the most biologically severe mass extinction in the Phanerozoic (Sepkoski, 1996; 2002). The most commonly cited cause of the end-Permian crisis is the Siberian Traps large igneous province (LIP), which may have released large volumes of greenhouse gases and other harmful volatiles to the atmosphere during volcanism and through contact metamorphism (Black et al., 2012; 2014; Burgess and Bowring, 2015; Ernst and Youbi, 2017; Jones et al., 2016; Svensen et al., 2009; Figure 1). The end-Permian extinction is marked by a sharp negative carbon isotope ($\delta^{13}C$) excursion (Baud et al., 1989; Magaritz et al., 1988; Shen et al., 2012), indicating an environmental disturbance that involved the potential release of ^{12}C-rich carbon to the ocean-atmosphere system (Figure 2). The end-Permian extinction was followed by a 5 Myr period of lingering recovery of the benthos (Hautmann, 2014; Hautmann et al. 2015) and of explosive recoveries interrupted by massive extinctions of the nekton (Brayard et al., 2009; Brayard and Bucher, 2015; Orchard, 2007). These diverging biodiversity patterns were accompanied by large positive and negative $\delta^{13}C$ fluctuations (Payne et al., 2004; Meyer et al., 2011; Grasby et al., 2016; Song et al., 2013), including at the Smithian/Spathian boundary (SSB) in the middle of the Early Triassic (Galfetti et al., 2007b).

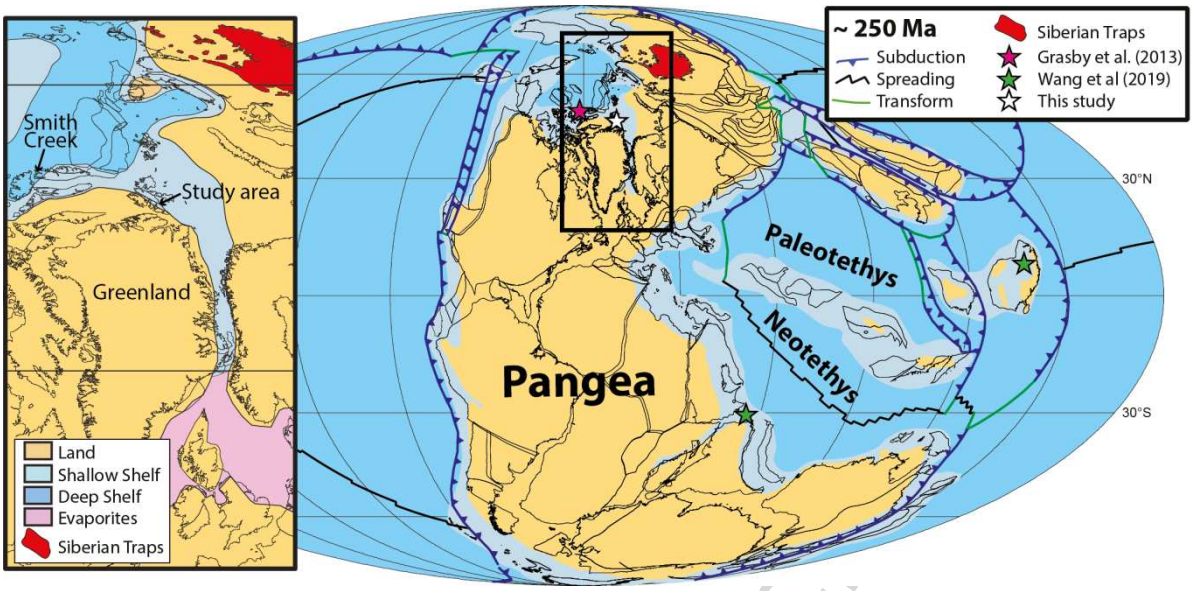

Figure 1. A paleogeographical reconstruction at around 250 Ma (Early Triassic), after Torsvik and Cocks (2017). Postulated plate boundaries are marked, with solid blue lines denoting subduction zones with teeth on the upper plate, black lines are spreading centres, and green lines are transform plate margins. Outlines of major crustal units are shown in black. Predicted paleoshorelines are from Golonka (2011). The known extent of the Siberian Traps LIP is shown in red. The pink star shows the sample locality used by Grasby et al. (2013), also the type locality of the Smithian substage at Smith Creek, Ellesmere Island. The green stars show the sample locations of Wang et al. (2019), while the white star shows the locality used in this study (see Figure 3).

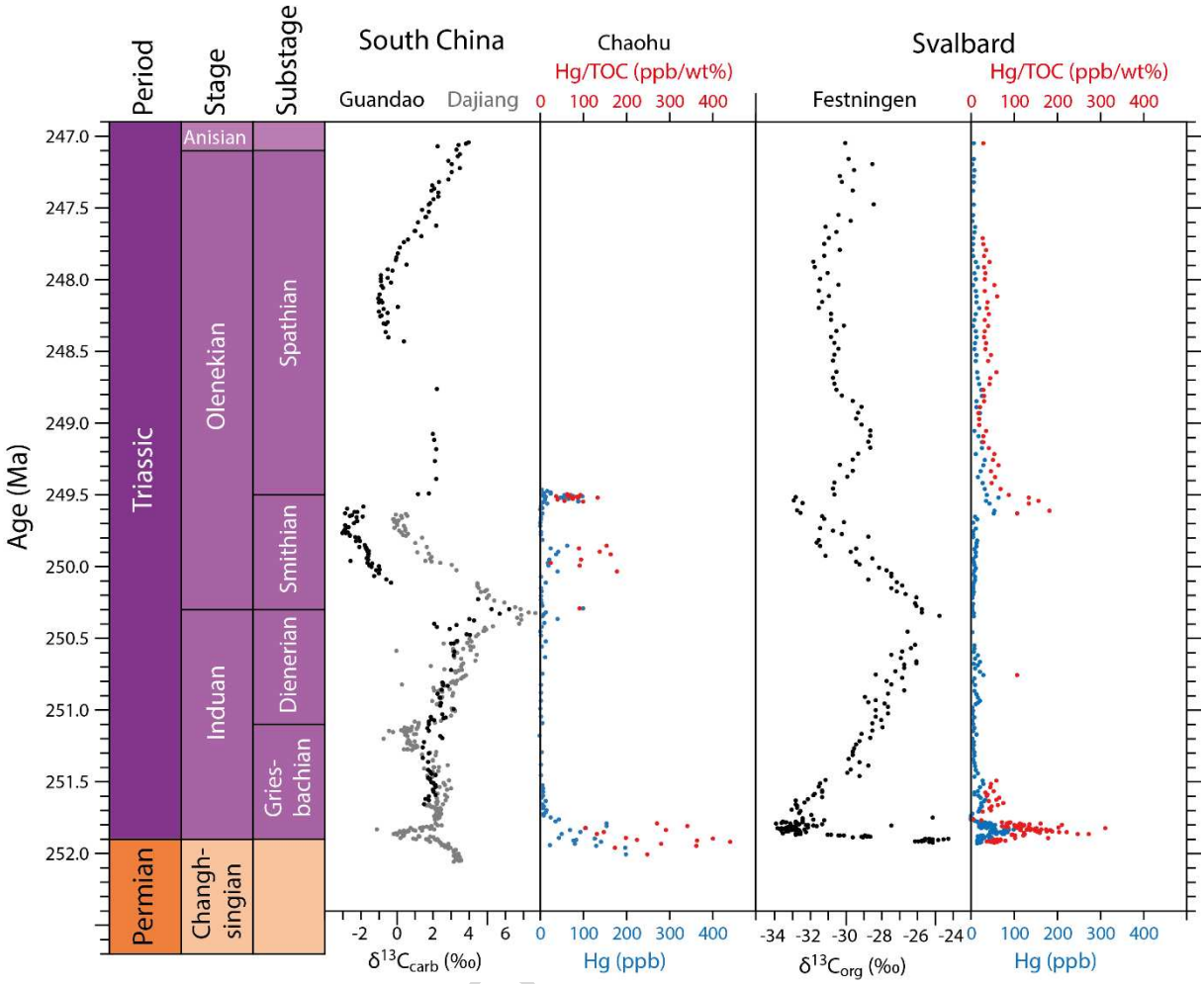

Figure 2. A summary of carbon isotope excursions and Hg anomalies in the Early Triassic. The South China $\delta^{13}C_{carb}$ data is from Meyer et al. (2011) and Payne et al. (2004), with the Guandao data points shown in black and the Dajiang data points shown in grey. Hg (blue) and Hg/TOC data from Chaohu are also shown (Wang et al., 2019). The Festningen $\delta^{13}C_{org}$, Hg (blue), and Hg/TOC (red) data from Svalbard are from Grasby et al. (2013; 2016). Hg/TOC values only shown where TOC >0.2 wt.% (Grasby et al. 2016), as TOC concentrations below this threshold result in errors in Hg/TOC values larger than any potential anomalies. These datasets have been calibrated with the latest generation of radio-isotopic ages (Burgess et al., 2014; Ovtcharova et al., 2015; Baresel et al., 2017). Constant sedimentation rates are assumed within each substage. Equal durations of the Griesbachian, Dienerian and Smithian substages are arbitrary because of the lack of radio-isotopic age dates. The duration of the Spathian is derived from the older generation of U-Pb ages (Galfetti et al., 2007b).

The Smithian was a period of intense carbon cycle instability, with a prolonged (100's kyr) and significant (4-10 ‰) negative $\delta^{13}C$ excursion (Figure 2; Payne et al., 2004; Tong et al., 2007). In contrast, the SSB is marked by a sharp positive $\delta^{13}C$ excursion (Payne et al., 2004) and a drastic extinction of marine nektonic organisms (Orchard, 2007; Brayard and Bucher, 2015). Wang et al. (2019) placed the SSB well after the onset of the CIE in South China, based on the first occurrence of the conodont index *Novispathodus pingdingshanensis*. However, the first occurrence of this species appears to be globally diachronous (Zhang et al., 2019), as it has been shown to co-occur with late Smithian taxa as well (e.g., *Xenoceltites*, Komatsu et al., 2016; Goudemand et al., 2012; Orchard & Zonneveld, 2009; *Glyptophiceras*, Romano et al., 2013; *Scythogondolella milleri*, Leu et al., 2018). The late Smithian extinction unfolded in a stepwise pattern, with a first diversity decrease of ammonoids during the early late Smithian *Wasatchites tardus* Zone (Brühwiler et al., 2010). It was followed by a further decrease during the late late Smithian *Glyptophiceras sinuatum* Zone (Brühwiler et al., 2010), where diversity was at its lowest (Brayard and Bucher, 2015), even lower than in the Permian-Triassic boundary bottleneck (Brayard et al., 2009). At least in the low paleolatitudes, ammonoids experienced an explosive re-diversification during the early Spathian (Brayard et al., 2006). The diversity of conodonts followed a roughly parallel trend (Orchard, 2007) and this clade experienced its last major evolutionary radiation from the SSB onward. Ecological communities of terrestrial plants were most profoundly affected during the middle Smithian as manifested by the presence of a spore spike (Hermann et al., 2011). Floras indicate a relatively more humid climate before the early late Smithian *W.tardus* Zone compared to drier climatic conditions during and after the same zone, but their ecological recovery was already well under way from the middle-late Smithian boundary on (Hermann et al., 2011; Hochuli et al., 2016). The composition of marine vertebrate apex predators was also reshuffled during the end-Smithian extinction, with the replacement of amphibians by reptiles (Scheyer et al., 2014).

Zhang et al. (2019) provided a thorough review of the available definition(s) of the SSB by means of ammonoids, conodonts, and carbon isotopes. In terms of ammonoids, these authors tacitly endorsed

the discrete and "natural" approach of biochronological boundaries as advocated by Lucas (2018), which was and still is successfully employed and refined in Early and Middle Triassic ammonoid biochronology. For the low latitudes, the current understanding in terms of ammonoids is that the SSB is within the interval of separation bounded by the *Glyptophyceras-Xenoceltites* zone below (Brühwiler et al., 2010) and the tirolitid n. gen. A beds above (Galfetti et al., 2007b). By no means does this definition exclude the future intercalation of one or several additional zones within this interval of separation. This can be anticipated from sections where the SSB global regression was outstripped by local tectonic subsidence (Bucher, ongoing work). However, this definition is not directly transferable to the high latitude record because: 1) correlatives of the late Smithian *Glyptophyceras-Xenoceltites* zone are always absent in the boreal record where it has been removed by the earlier onset of the SSB gap, and 2) the explosive diversification of tirolitids is restricted to low latitudes. Our recent finding of the oldest tirolitid (= tirolitid n. gen. A in Galfetti et al. 2007b) associated with *Bajarunia euomphala* in Nevada (Bucher, ongoing work) combined with the here newly reported occurrence of *B. euomphala* 0.60 m above the base of the Vendomdalen Member at Stensiöfjellet considerably narrows down the interval of separation containing the SSB in the Spitsbergen record. There, the SSB is now bracketed by the top of the *Wasatchites tardus* Zone below and the new base of the *Bajarunia euomphala* Zone above.

In terms of conodont Unitary Association zones, ongoing work by Leu et al. in several low latitude records leads to improved accuracy and precision, but this is not directly relevant to the Spitsbergen data presented here which rely on ammonoid age control.

Last but not least, the utilization of the carbon isotope record as a surrogate in the absence of age-diagnostic fossils is directly dependent on the completeness of the record and sedimentation rates. Considering the evidence for a global regression straddling the paleontologically defined SSB, great care is needed when attempting detailed chemostratigraphic correlations during the late Smithian and basal Spathian. We also presently document that the onset of the positive CIE is still within the

middle Smithian in Spitsbergen, thus newly highlighting an earlier inception of the CIE in the high latitudes. We additionally confirm that in Spitsbergen, the positive maximum of the CIE is within the basal Spathian.

Several studies have suggested the occurrence of late-phase volcanic activity of the Siberian Traps around the time of the SSB as a cause for "lethally" hot climate (e.g. Paton et al., 2010; Orchard 2007; Xie et al., 2010; Sun et al., 2012; Shen et al., 2019a). However, these studies rest on age controls that have been cast into doubt by recent literature, especially the hypothesis that the first occurrence of the conodont index *Novispathodus pingdingshanensis* is a synchronous marker defining the base of the Spathian (Goudemand et al., 2013; Zhang et al., 2019). Some other studies with correct age control also suggested that acidification through volcanogenic volatiles may have contributed to the late Smithian extinction (Galfetti et al. 2007). At present, the available radiometric ages of the Siberian Traps basalts are confined to close to the Permian-Triassic boundary (Burgess et al., 2014; Kamo et al., 2003). This may be a sampling bias due to the focus on this key horizon as over 1000 m of Early Triassic flows post-date this sequence (Kamo et al., 2003). Therefore, while there is evidence of continued Siberian Traps volcanism after the Permian-Triassic boundary, there are currently no time constraints on these eruptions and no direct evidence of elevated volcanic activity around the SSB.

One method used as a proxy for major volcanism in sedimentary sequences that has received considerable recent attention is the use of mercury (Hg) anomalies (Sanei et al., 2012). Mercury deposition is primarily driven by complexation with organic matter, such that a strong positive correlation exists between Hg and total organic carbon (TOC) in many sedimentary sequences (Outridge et al., 2007; Ruiz and Tomiyasu, 2015; Sanei et al., 2014). It is assumed that positive anomalies of Hg/TOC values occur when elevated Hg emissions are released into the environment, resulting in alternate modes of Hg deposition to organic matter drawdown, such as in sulfides or adhered to clays (Sanei et al., 2012; Shen et al., 2019b). Volcanic activity is one of the primary

atmospheric Hg sources in the present time (Pyle and Mather, 2003). Therefore, sharp increases in Hg/TOC values preserved in the sedimentary record have been traditionally interpreted as a proxy for enhanced volcanism. Hg/TOC anomalies have been reported from several of the major environmental crises, including the end-Permian (Sanei et al., 2012; Grasby et al., 2013; 2016), end-Triassic (Thibodeau et al., 2016; Percival et al., 2017), Cretaceous-Paleogene (Sial et al., 2013; Font et al., 2016; Keller et al., 2018) and the Paleocene-Eocene (Keller et al., 2018; Jones et al., 2019).

However, several recent studies have suggested Hg/TOC anomalies can be caused by non-volcanic factors. Clay mineral surfaces and sulfides can also host Hg (Ravichandran, 2004; Selin, 2009), so conditions that favour Hg-uptake into these fractions may be important. Measurements across Jurassic and Cretaceous Oceanic Anoxic Events (Percival et al., 2018; Them II et al., 2019) suggest that Hg/TOC anomalies correlate with proximity to paleoshoreline, potentially indicative of clay-hosted Hg (Them II et al., 2019). The redox properties of depositional waters are also a key factor, as reducing conditions favour the formation of HgS and incorporation of Hg into iron sulfides (Bower et al. 2008, Duan et al., 2016). Euxinic conditions appear to favour sulfide-hosted Hg over organic-hosted Hg, which can create the appearance of Hg/TOC anomalies in pyrite-dominated successions such as in Ordovician/Silurian boundary sections (Shen et al., 2019b). Finally, changes to organic matter sourcing can result in apparent Hg/TOC 'anomalies', due to variations in Hg-uptake into organic matter in numerous marine and terrestrial ecosystems (Percival et al., 2018; Jones et al., 2019). It is therefore of great importance to investigate multiple sections across a specific time interval to gain a true understanding of the origins of any Hg/TOC anomalies in marine sediments (Them II et al., 2019; Jones et al., 2019).

In the case of the SSB marine extinction and associated ecological turnover of floras, a detailed stratigraphic relationship between Hg/TOC anomalies, anoxia, organic matter, and the distribution of global stratigraphic gaps is required to fully assess the possibility of volcanism as a primary trigger of the environmental disturbances. Several studies have published Hg/TOC variations through the Early

Triassic (Figure 2). Grasby et al. (2013) measured Hg/TOC values at Smith Creek, Sverdrup Basin, Arctic Canada (Figure 1), which is the type section of the Smithian substage (Tozer, 1967). Modest Hg/TOC anomalies are recorded from the middle Smithian (Figure 2), which overlap with the onset of the large negative $\delta^{13}C$ excursion (ca. 470 to 550 m). Background Hg/TOC values are observed in the early late Smithian and across the SSB, with a brief return to modest Hg/TOC anomalies in the early Spathian (ca. 590 to 610 m; Fig. 3 in Grasby et al., 2013). At Smith Creek (Tozer, 1967), late Smithian ammonoids occur in a somewhat condensed carbonate horizon near 570 m and are exclusively assigned to the early late Smithian *Wasatchites tardus* Zone. Together with the very abrupt lower flank of the positive carbon isotope excursion, it strongly suggests the presence of a hiatus straddling the latest Smithian (*Glyptophiceras sinuatus* Zone of Brühwiler et al., 2010). Subsequently, Grasby et al. (2016) described extensive geochemical records from the Permian Kapp Starostin Formation up to the Spathian Tvillingodden Formation at Festningen, western Spitsbergen. This locality represents a near-shore, shallow water setting (Mørk et al., 1982; Wignall et al., 2016) that lacks adequate biostratigraphic control. There are pronounced Hg/TOC anomalies that begin close to the peak of the late Smithian negative $\delta^{13}C$ excursion and continue to the peak of the positive $\delta^{13}C$ excursion of the early Spathian (Figure 2). These results and interpretations stand in marked contrast with the Tethyan SSB records from Guryul (Kashmir) and Chaohu (South China), which do not reveal any clear Hg/TOC anomaly concomittent with the late Smithian positive CIE (Wang et al., 2019). However, a limiting factor with both of these data sets (Grasby et al., 2016; Wang et al., 2019) is that TOC concentrations for much of the Early Triassic are extremely low in these sections (Figure 2). The recommended limit for interpreting Hg/TOC concentrations is 0.2 wt% (Grasby et al., 2016), with errors below this arbitrary threshold considered greater than potential Hg/TOC anomalies. While the latest Smithian Hg/TOC values appear to be anomalously high compared to early Spathian strata (Figure 2; Grasby et al., 2016; Wang et al., 2019), it is not possible to assess whether these elevated latest Smithian Hg/TOC values are an isolated event. It is possible that similar Hg/TOC values are present in mid Smithian sections with higher TOC concentrations.

Here, we report on the mercury record, organic carbon isotope, and trace element data across the Smithian-Spathian boundary at Wallenbergfjellet in central Spitsbergen. This represents a more distal (offshore) depositional setting to the Festningen section (Grasby et al., 2016), with adequate biostratigraphic age control.

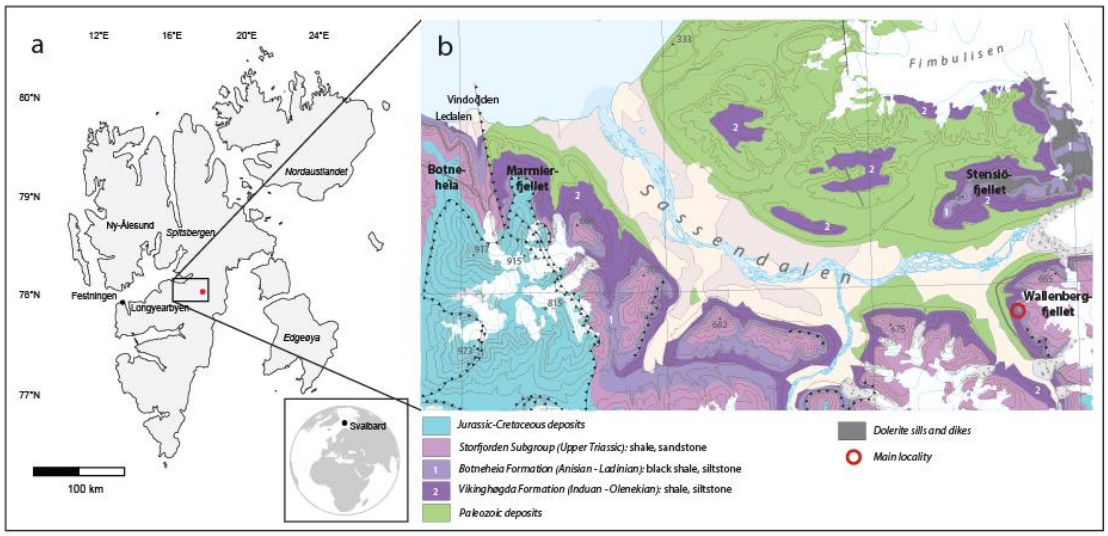

Figure 3. Map of Svalbard with the studied locality at Wallenbergfjellet, Spitsbergen. a) The location of the study area and the Festningen site used by Grasby et al. (2016). b) Geology of the study area, lithologies are redrawn from geological maps of Svalbard (Major et al., 2001).

2. Geological setting and age controls

A geological map of the study area is shown in Figure 3. In central Spitsbergen the Lower Triassic succession is stratigraphically defined as the Vikinghøgda Formation, which represents an offshore (> 50 km from shore, e.g. Wignall et al. 2016) shelf environment that is the distal continuation of the coastal and shallow marine deposits of the time equivalent Vardebukta and Tvillingodden formations of western Spitsbergen (Festningen section). The lower member of the Vikinghøgda Formation, the Deltadalen Member, is Griesbachian to Dienerian in age and equivalent to the Vardebukta Formation. The Lusitaniadalen and Vendomdalen members roughly represent the Smithian and Spathian

substages and are time equivalent to the Tvillingodden Formation (Mørk et al., 1999; Wignall et al., 2016). The Vikinghøgda Formation is a deposit of sandy silts grading into silty grey shales and silty black shales. Horizons of calcareous nodules and calcareous paper shale are widespread in the Lusitaniadalen and Vendomdalen members. The formation was deposited on a gently sloping marine ramp during stepwise deepening (Mørk et al. 1999; Wignall et al. 2016). The stratigraphic boundary between the Lusitaniadalen Member and the Vendomdalen Member is defined as the top of a yellow-weathering cemented sandstone (Mørk et al., 1999). The level roughly corresponds to a shift from grey shale to dark grey paper shale, which is often apparent in the field. At Wallenbergfjellet, the shift to dark grey paper shale was in some places found to overlie the defined boundary with a few tens of centimeters.

Brühwiler et al. (2010) first established that the latest Smithian *Glyptophiceras sinuatum* Zone overlies the early late Smithian *Wasatchites distractus* Zone in recently studied Tethyan sections from the northern Indian margin. The same succession has been subsequently confirmed in several sections of the western USA basin (Jattiot et al., 2017; Jenks and Brayard, 2018). The *W. distractus* Zone and the *G. sinuatum* Zone correlate with the lower and the upper parts of the more comprehensive *Anasibirites multiformis* beds as initially described by Brayard and Bucher (2008) in the Nanpanjiang Basin. The *A. multiformis* Zone of these authors was synonymous with the entire late Smithian record preserved in South China, but ongoing work indicates that in fact, the *W. distractus* and the *G. sinuatum* zones consistently occur in superposition within the late Smithian black shales of the Nanpanjiang Basin, in perfect agreement with other sections from the northern Indian margin and the western USA. Therefore, the scope of the low paleolatitude *A. multiformis* Zone must be reduced to the first zone of the late Smithian (Jattiot et al., 2015). The *A. multiformis* Zone is a strict correlative of the *W. distractus* Zone in the high latitudes. Hence, the low paleolatitude records show that the *G. sinuatum* Zone systematically occurs within the upper half of the late Smithian positive CIE, immediately preceding the heaviest values and the abrupt return to lighter values in the early Spathian. The boundary between the Smithian and Spathian substages in

the Boreal Realm was defined by the last occurrence of the ammonoid *Wasatchites tardus*, which is the oldest of the two late Smithian ammonoid zones (Brühwiler et al., 2010). This definition avoids the fact that the paleontological boundary between the Smithian and the Spathian is within a longer gap whose base includes the *G. sinuatum* Zone in the Sverdrup Basin, in northern Siberia, in NE British Columbia and in Spitsbergen. The onset of the global late Smithian gap is thus earlier in the Boreal record than within the Tropics.

A widely used proxy for the Smithian/Spathian biostratigraphic boundary is the presence of a global positive $\delta^{13}C$ excursion. In Dicksonland, central Spitsbergen, Galfetti et al. (2007a) first established that the end of the positive CIE is within the lower part of the Vendomdalen Member. At variance with their earlier paper on the Sverdrup Basin (Grasby et al., 2013), Grasby et al. (2016) placed the SSB at Festningen, western Spitsbergen, at the minimum of the $\delta^{13}C$ curve, i.e. at the base of the onset of the positive $\delta^{13}C$ excursion, and in coincidence with the Hg/TOC anomalies. However, this placement of the boundary with respect to the CIE at Festningen (Grasby et al., 2016) is in conflict with other data. In the Tethyan ammonoid and carbon isotope records (Brühwiler et al., 2010; Galfetti et al., 2007b), the substage boundary is rather associated with the end of the ascending limb of the positive CIE. Even if the *G. sinuatum* Zone corresponds to a gap in the Boreal record, the isotope records from Dicksonland (Galfetti et al., 2007a) demonstrate that the maximum of the positive CIE is within the lower part of the Vendomdalen Member, which is of early Spathian age, and that it has a gently gradual shape, not a spike shape like in most low latitude records. At Wallenbergfjellet, the end of this positive CIE is also found in the lower part of the Vendomdalen Member, whose age is not well constrained in terms of ammonoids. However, at Stensiöfjellet (only 5 km north of Wallenbergfjellet) where the stratigraphic sequence is similar, we found a basal Spathian ammonoid fauna characterized by *Bajarunia euomphala* 60 cm above the base of the Vendomdalen Member, i.e. within the maximum of the positive CIE.

Thick sills of Early Cretaceous age (the Diabasodden Suite) were emplaced into the Triassic succession throughout central Spitsbergen. At Wallenbergfjellet, a large intrusion, locally expressed as a 10 m thick dyke, crops out a few hundred meters away from the studied section. It is possible that this dyke is connected to a sill underlying the section of similar thickness to the dyke. Based on the uninterrupted stratigraphic succession for at least 100 m below our studied interval we assume that such a sill has not disturbed the geochemistry to any serious degree. In the Upper Triassic at Botneheia in Central Spitsbergen, Hubred (2006) reported little thermal effect on organic matter outside an aureole of ca. 1.5 times the sill thickness.

3. Material and methods

3.1. Sampling

In 2017 we collected 48 shale samples from the Wallenbergfjellet section, from 18 m below the base of the Vendomdalen Member to the base of the overlying Botneheia Formation (Anisian). The section was sampled at 2 m intervals, with the exception of the interval from 6 m below to 4 m above the base of the Vendomdalen Member, which was sampled at 1 m intervals (Figure 4). We collected ammonoids from throughout the section, although the lower part of the Vendomdalen Member yielded only few and poorly preserved specimens. Some ammonoids reported in Figure 4 were found in adjacent sections with the same lithological development.

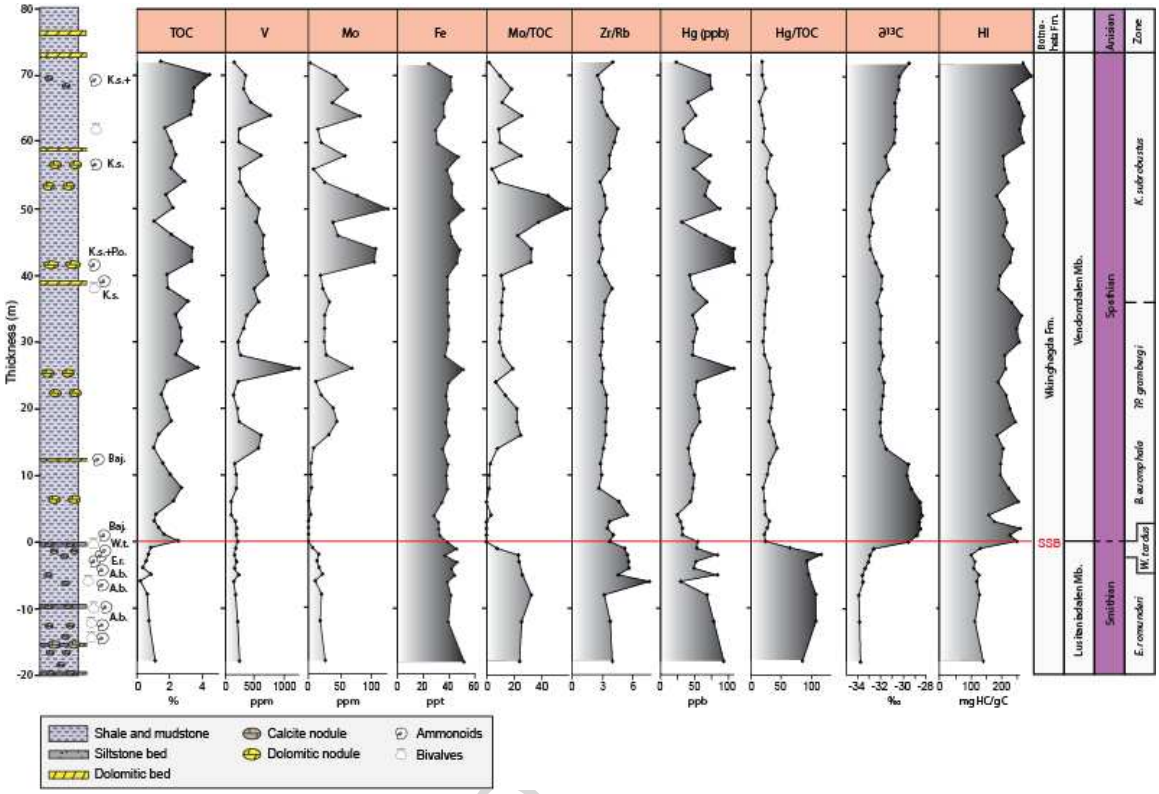

Figure 4. Lithological log, biostratigraphy and geochemical logs from the Wallenbergfjellet section. Two samples (-6 and -4 m) had TOC < 0.5 %, and Mo/TOC and Hg/TOC were therefore discarded (Them II et al., 2019). Some ammonoids in the Vendomdalen Member were found in adjacent sections. Ammonoids listed are A. b.: *Arctoceras blomstrandi*; E. r.: *Euflemingites romunderi*; W. t: *Wasatchites tardus*/*Xenoceltites* spp./*Anasibirites kingianus* assemblage; Baj.: *Bajarunia* sp.; K. s.: *Keyserlingites subrobustus*; P. o.: *Popovites occidentalis*; K. s.+: *K. subrobustus*/*Svalbardiceras spitzbergensis*/*S. freboldi*?/*P. occidentalis*/*Pseudosageras* sp./*Procarnites* sp. assemblage.

3.2. Mercury analysis

Mercury analysis was conducted at the University of Oxford using the Lumex RA-915 Portable Mercury Analyser with a PYRO-915 pyrolyzer (Bin et al., 2001). Analytical procedures followed in-

house protocols (Percival et al., 2017; Jones et al., 2019), where between 40-60 mg of powdered sample was weighed before being transferred to the pyrolyzer and heated to 700 °C. Sample peaks in the spectrometer were calibrated using the NIMT/UOE/FM/001 peat standard with a known Hg concentration of 169 ±7 ppb, with repeat calibrations every ten samples to negate any drift in the instrument. Each sample was run in duplicate, which resulted in an analytical error of ±5 %.

3.3. Handheld XRF and SEM-EDX

Flat pieces were selected from each sediment sample, washed and analysed using handheld X-ray fluorescence spectroscopy (HHXRF). The instrument used was a Thermo Scientific Niton XL3t GOLDD+ with an aperture of 8 mm. Integration time was 120 s in the "Mining Cu/Zn" mode. After every five samples, a calibration measurement was taken on a pressed powder pellet of the USGS Columbia River Basalt BCR-2 standard, diluted to four parts powder and one part binder. The diluted standard has a certified V concentration of 416 ± 14 (1 σ) ppm. No drift in the V measurement of the standard was observed, and the variance was relatively small, with average V concentration 420 ± 24 (1 σ) ppm, N = 10, i.e. within the error of the certified standard value. Using the same instrument model, Schovsbo et al. (2018) reported excellent correlation between HHXRF and ICP-MS values for V and Mo in dark shales (R^2 = 0.98 and R^2 = 0.96, respectively) over wide ranges. Still, we regard the V, Mo, Fe and Zr/Rb curves obtained as semi-quantitative.

SEM and EDX microimaging was carried out on selected samples to investigate distributions of iron and pyrite, using a Hitachi S-3600N SEM in the backscatter (BSE) mode and with a Bruker XFlash 5030 energy dispersive X-ray detector (EDX), at the Natural History Museum in Oslo.

3.4. Organic geochemistry

Total organic carbon content (TOC) was measured by Applied Petroleum Technology, Oslo, Norway, with a Leco SC-632 instrument. Diluted HCl was added to the powdered sample to remove carbonate. The sample was then introduced into the combustion oven, and the amount of carbon was measured

as carbon dioxide by an IR-detector. Rock-Eval pyrolysis used the Rock-Eval 6 instrument at 300 °C for 3 min, increasing by 25 °C/min to 650 °C. The Jet-Rock 1 standard was run as every tenth sample and checked against the acceptable ranges according to the Norwegian Industry Guide to Organic Geochemical Analysis (NIGOGA), 4th edition.The permissible range for TOC in the Jet-Rock standard is 11.3-12.5 %.

3.5. Bulk organic carbon isotope analysis

Carbon isotope analysis was carried out at Liverpool University. Approximately 0.5 g of powdered sample was weighed into a glass beaker and carbonate minerals (and other acid soluble phases) were removed by reaction with 40 ml of 1M HCl (pH 0.0) at 35 ^{o}C for 24 h. Following decomposition the acid insoluble residue was recovered by centrifugation, washed free of any remaining acid by repeated cycles of rinsing with deionised water, and freeze-dried.

Carbon dioxide for mass spectrometric measurement of carbon ($^{13}C/^{12}C$) isotope ratios in samples of organic carbon was prepared using a modification of the classical 'sealed tube' combustion procedure described by Frazer and Crawford (1963) and Sofer (1980). Decarbonated (1M HCl, 35 ^{o}C, 24 h) bulk sediment samples (sufficient to yield ~100 μmols of CO_2) were weighed into silver foil capsules and loaded into pre-conditioned (650 ^{o}C, 24 hrs) quartz tubes together with 3 g of Cu(II)O and 0.5g of Cu metal. All tubes were then sealed under vacuum and organic carbon was converted to CO_2 by combustion at 850 ^{o}C for 2 hrs. Following combustion the tubes were allowed to cool to 600 ^{o}C (and held for 4 hrs) in order to allow conversion of any nitrous oxide (in contact with Cu metal) to nitrogen before final cooling (~16 hrs) to room temperature.

Product CO_2 was recovered under vacuum using standard cryogenic separation procedures (to remove H_2O and N_2) and the amounts of the component masses (*m/z* 44, *m/z* 45, *m/z* 46) were measured with respect to a comparison (reference) CO_2 using a VG SIRA 10 dual-inlet, gas source

mass spectrometer. Resultant delta values ($\delta_{CO_2}^{45/44}$ and $\delta_{CO_2}^{46/44}$) were subsequently corrected for ^{17}O contributions (Craig, 1957), and calibrated to the Vienna Pee Dee Belemnite (VPDB) carbon isotope scale *via* measurement of CO_2 prepared from multiple aliquots of an in-house Carrara marble (LIVM2) calcite ($10^3\delta^{13}C_{VPDB}$= +1.98) and a polyethylene (IAEA-CH7) international reference material ($10^3\delta^{13}C_{VPDB}$= -32.15) run with each batch of unknowns. Isotopic ratios are reported as conventional delta values with respect to the VPDB scale ($\delta_{OC}{}^{13}C_{VPDB}$)

All sample data were normalized against LIVM2-CH7 such that $\Delta_{LIVM2\text{-}CH7}$= 34.13‰. Analytical precision (2σ) is estimated to be better than ±0.1 ‰ based on the replicate measurement of IAEA-CH7.

Data were plotted and analyzed with the software Past, v. 3.18 (Hammer et al., 2001).

4. Results

4.1. Ammonoid biostratigraphy

The lithological log, biostratigraphy and geochemistry are shown in Figure 4. Ammonoids were collected from carbonate nodules and lenticular horizons throughout the section. Ammonoids identified at -4.3 m and below in the section are mostly *Arctoceras* cf. *blomstrandi* and *Juvenites spathi* belonging to the comprehensive *E. romunderi* Zone of middle Smithian age. *Euflemingites* itself was found at -3.0 m, and *Juvenites spathi* at -2.0 m. At -1.3 m, -1.2 m and immediately below the base of the Vendomdalen Member, an abundant ammonoid fauna from the *W. tardus* Zone (early late Smithian) was recovered, with *Wasatchites tardus*, *Xenoceltites* spp., *Arctoprionites* sp. and *Anasibirites kingianus*. The *W. tardus* Zone is therefore recognized from ca. -2.0 m to the top of the Lusitaniadalen Member.

Ammonoids are more scattered and generally poorly preserved in the Vendomdalen Member. A *Bajarunia* sp. indet. at 12 m is indicative of the *B. euomphala* Zone, early Spathian. *Keyserlingites subrobustus* was found from 39 m almost to the top of the Vendomdalen Member, documenting a thick late Spathian *K. subrobustus* Zone. An interval with small, gray carbonate nodules near the top of the member contains a rich, well-preserved late Spathiancephalopod fauna (cf. Mørk et al., 1999) with *K. subrobustus*, *Svalbardiceras spitzbergensis*, *S. freboldi*?, *Popovites occidentalis*, *Pseudosageras* sp., *Procarnites* sp. and orthocone nautiloids.

4.2. Carbon and trace element geochemistry

TOC values are low (< 1.2 wt.%) in the Lusitaniadalen Member (Figure 4). In the Vendomdalen Member the TOC is variable but higher, averaging 2.3 wt.% and reaching 4.4 wt.% in the upper part. Vanadium content is below 270 ppm in the Lusitaniadalen Member and the lower 12 m of the Vendomdalen Member. The upper part of the Vendomdalen Member has variable but higher V content, with an average of 450 ppm. Molybdenum shows a similar pattern as V, with values below 30 ppm up to 12 m, then increasing to an average of 44 ppm in the upper part. Average 2σ precision (repeatability) on V across all samples is 48 ppm, on Mo 2.6 ppm.

Zr/Rb values are generally below 4 in most of the section, but with elevated values (up to ca. 7) from -6 to +6 m. As zirconium is more prevalent in coarser, lithic grains and rubidium binds preferentially to clay particles, the Zr/Rb can be used as a proxy for grain size (Dypvik and Harris, 2001). The higher Zr/Rb values around the Lusitaniadalen-Vendomdalen member boundary therefore indicate coarser grain size, compatible with a more proximal depositional setting.

The vanadium values throughout the Wallenbergfjellet section are much higher than the 50 ppm reported from the Early Triassic of Western Spitsbergen by Wignall et al. (2016), but this difference is probably due to higher aluminium content in the more distal, finer-grained facies at this locality. Vanadium is a redox sensitive element (e.g., Tribovillard et al, 2006), indicating relatively more oxygenated bottom water conditions in the -18 m to +12 m interval than in the upper part of the

section. This is supported by low (< 1.5%) TOC values in the Lusitaniadalen Member, although TOC increases to almost 3% already at the base of the Vendomdalen Member. V and TOC are positively correlated through the section (R=0.48, p<0.001, N=48). Molybdenum shows the same pattern, correlating strongly with V (R=0.65, p<0.001, N=48).

The Niton HHXRF is known to be imprecise for light elements, and Schovsbo et al. (2018) found very poor correlation with ICP-MS data for Al. We do therefore not present curves for V/Al, Mo/Al or Hg/Al. However, the lithology does not vary strongly through our section, and also the measured Al values vary within only a small range (ca. 6 to 8 %). Normalization for Al would therefore probably not change the general trends to any large degree.

Molybdenum is generally a redox sensitive element (Tribovillard et al., 2006), although only very high Mo values (> 25 ppm) can be used to infer euxinic conditions, while lower values cannot be interpreted unambiguously with respect to redox conditions (Hardisty et al., 2018).

The hydrogen index (HI) from the Rock-Eval analysis is consistently below 140 (~120 on average) in the Lusitaniadalen Member, suddenly increasing to above 160 (~225 on average) in the Vendomdalen Member (Figure 4). The oxygen index (not shown) shows the opposite pattern, with high values (average 120) in the Lusitaniadalen Member decreasing to an average of 30 in the Vendomdalen Member. The sudden increase in the hydrogen index at the base of the Vendomdalen Member is in accordance with the results of Mørk et al. (1999), who noted a shift in type of organic matter from type III kerogen (i.e. of more terrestrial origin) to mixed type II/III at the same stratigraphic level. This was accompanied by a reduction in terrestrial palynodebris and a shift to mainly marine plankton (Mørk et al., 1999). Our preliminary, high-resolution palynological investigations from Wallenbergfjellet do not indicate a sudden, clear increase in marine organic matter across the SSB that matches the rapid shift in Rock-Eval values. Another possible mechanism for the increase in hydrogen index is decreased oxidation and/or decreased bioturbation (e.g., Durand and Monin, 1980) in the less oxic (higher TOC) facies of the Vendomdalen Member.

The organic $\delta^{13}C$ curve shows rather negative values in the Lusitaniadalen Member (between -33.84 and -32.55 ‰) with a slight positive trend in the upper part (Figure 4). An abrupt positive shift to -29.53 ‰ at the base of the Vendomdalen Member marks the onset of a positive excursion in the interval from 0 to 11.7 m. Isotope values remain fairly stable around -32 ‰ until about 40 m in the section, followed by a slight negative excursion and a trend towards more positive values from ca. 50 m to the formation top. Interestingly, the gradual onset of the positive CIE starts in the middle Smithian (Figure 4), which suggests a somewhat earlier inception than in the low paleolatitudes. The smooth end of the positive CIE is 3-4 m above the base of the Vendomdalen Member, in agreement with the record from Dicksonland, Spitsbergen (Galfetti et al., 2007a), although the coarser sampling from Dicksonland does not allow restoring the gradual and smooth shape of the end of the excursion.

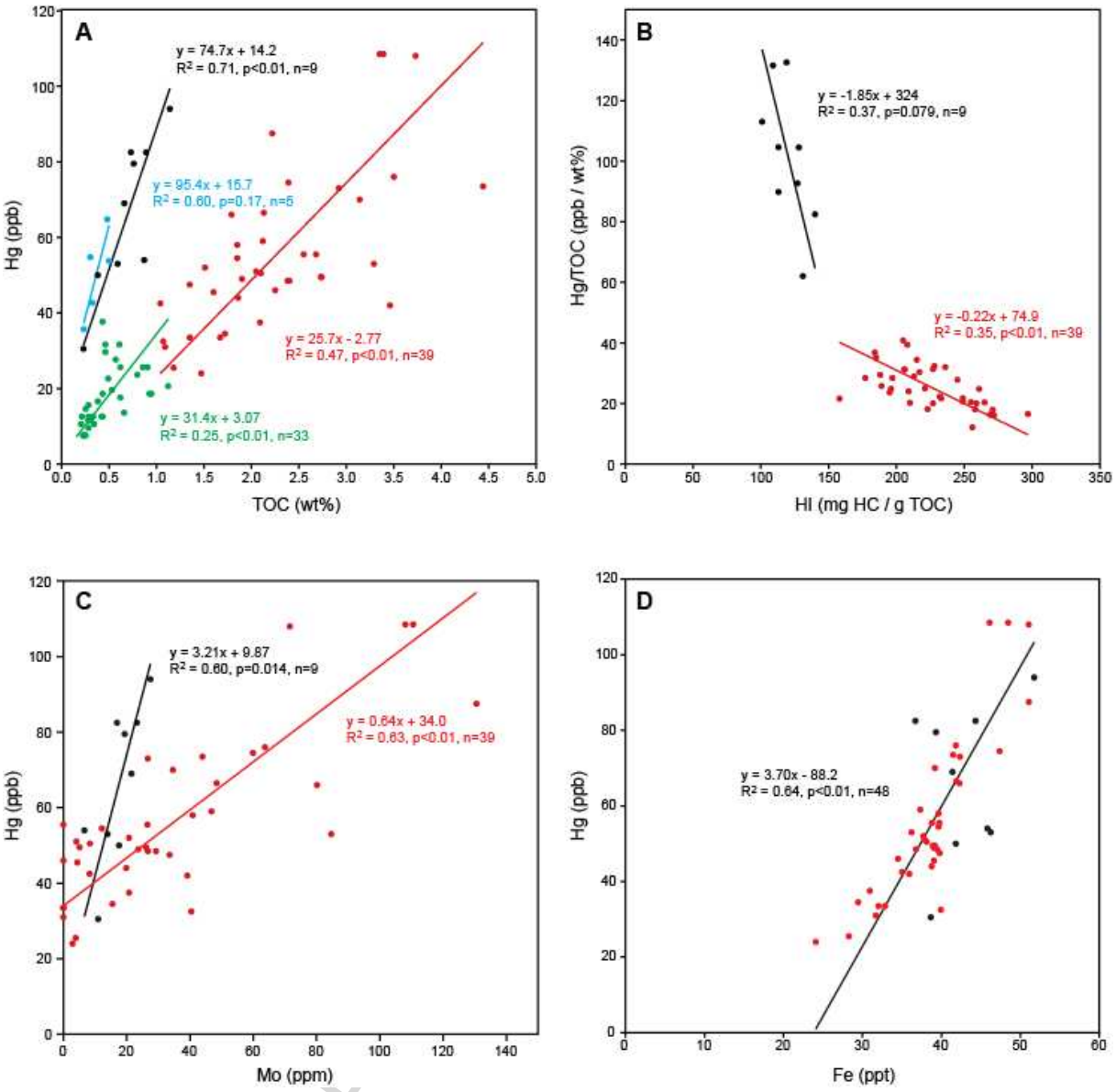

Figure 5. A: Cross plot of total organic content (TOC) versus Hg. Black: Smithian samples (below 0 m in the section; Lusitaniadalen Mb.) at Wallenbergfjellet, central Spitsbergen (this study). Red: Spathian samples (above 0 m; Vendomdalen Mb.) at Wallenbergfjellet. Blue: Smithian at Festningen, western Spitsbergen, data from Grasby et al. (2016). Green: Spathian at Festningen. Regression lines are based on the RMA method; *p* values computed by permutation test on R^2. Slopes are significantly different between the Smithian and Spathian (χ^2=11.7, p<0.01). Slopes are not significantly different between Wallenbergfjellet and Festningen. B: Hydrogen index (HI) versus Hg/TOC in the Smithian (black) and Spathian (red) at Wallenbergfjellet. C: Molybdenum (Mo) versus Hg in the Smithian (black) and the Spathian (red) at Wallenbergfjellet. D: Fe versus Hg in the Smithian (black) and Spathian (red) at Wallenbergfjellet.

4.3. Mercury

Mercury concentrations range from 24 to 109 ppb throughout the section. Although these values are relatively low, they are generally about two times higher than the nearshore locality in western Spitsbergen (Grasby et al., 2016). Mercury concentrations are highest in the Lusitaniadalen Member and sporadic parts of the upper Vendomdalen Member (Figure 4). However, normalizing to TOC shows a completely different picture with anomalously high Hg/TOC values (62–132 ppb/wt%) in all Lusitaniadalen Member samples. In contrast, all Vendomdalen Member samples have low Hg/TOC values (12–41 ppb/wt%). As shown in Figure 5A, there is strong correlation between TOC and Hg in both Spitsbergen localities, but with considerably higher regression slope in the Lusitaniadalen Member than in the Vendomdalen Member. The largest Hg/TOC values are documented in the interval from -6 to -2 m in the section. The plateau-like Hg/TOC anomaly of the Lusitaniadalen Member is present throughout the middle Smithian, as indicated by the ammonoid age control. The Hg/TOC anomaly decreases within the early late Smithian and reached background values during the early Spathian at the latest (Figure 4). The Hg/TOC and $\delta^{13}C$ curves appear discontinuous at this level, supporting the presence of a hiatus in the uppermost Smithian (i.e. the missing *G. sinuatus* Zone). The observation that the Hg/TOC anomaly largely precedes the positive CIE is in agreement with the record obtained from a more proximal setting in West Spitsbergen as analysed by Grasby et al. (2016). Therefore, this dataset suggests that a clear and sustained Hg/TOC anomaly was present in the middle Smithian, which had disappeared by the early Spathian. TOC concentrations in the Choahu section (Wang et al., 2019) are too low in the mid to late Smithian to allow meaningful analyses of whether Hg/TOC anomalies are present (Figure 2).

Iron is present at 25-50 ‰ throughout the section (Figure 4). In the Smithian, SEM-EDX images indicate that Fe is present both in euhedral pyrite and clastic mineral grains (Figures 6A, C). In the Spathian, Fe is largely confined to euhedral and framboidal pyrite (Figures 6B, D).

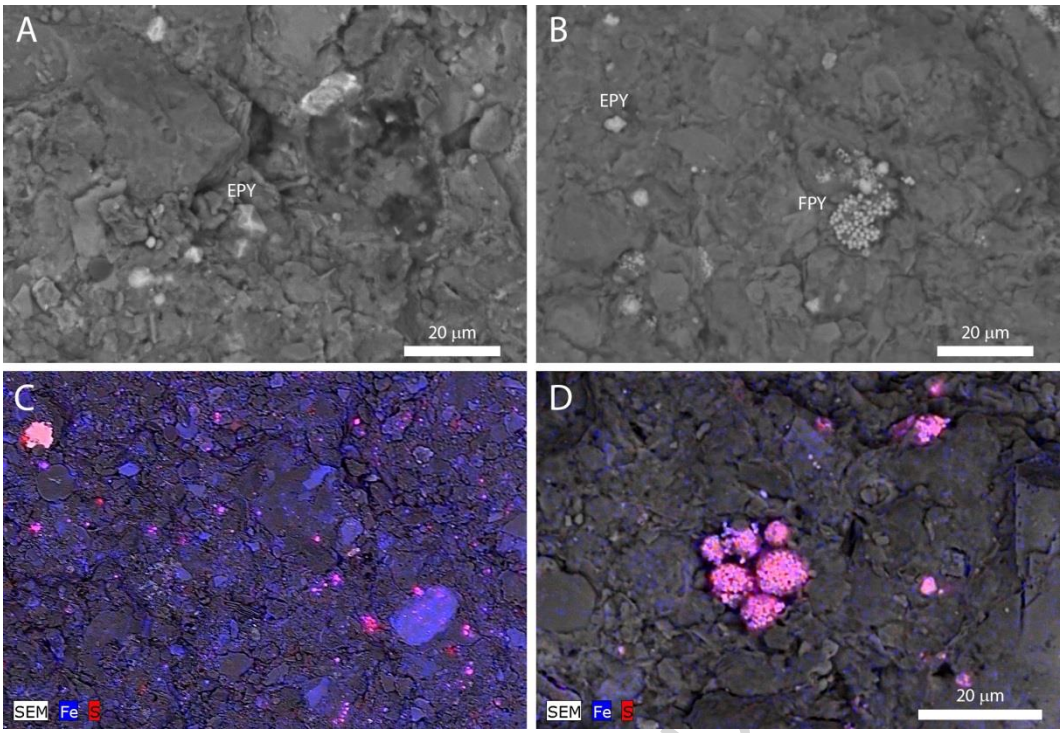

Figure 6. SEM-EDX images from the Wallenbergfjellet section: A: BSE image from -18 m in the section (Smithian). Note euhedral pyrite (EPY). B: BSE image from 60 m (Spathian). Note euhedral (EPY) and framboidal (FPY) pyrite. C: BSE and element map (EDX) image showing distribution of Fe (blue) and S (red) at -18 m (Smithian). Iron is found both in scattered euhedral pyrite grains and in other minerals. D: BSE and element map image from 60 m (Spathian), showing well-developed framboidal pyrite, with little Fe in the matrix.

5. Discussion

The comparison of the Wallenbergfjellet SSB section and the Festningen section of Grasby et al. (2016) strongly suggests the presence of a latest Smithian gap in Spitsbergen. This gap may be coeval with that of the Sverdrup Basin (Smith Creek; Grasby et al., 2013). In both basins, the latest Smithian *G. sinuatum* Zone is missing. In the well-studied ammonoid record from northern Siberia (Dagys, 1994) and NE British Columbia (Tozer, 1994), the only documented late Smithian zone is the *W. tardus* Zone, which consistently suggests an earlier onset of the gap on shelves in Siberia, the

Canadian Arctic, NE British Columbia and Spitsbergen. This timing contrasts with the majority of low paleolatitude SSB sections where the *G. sinuatum* Zone is found above the *A. multiformis* Zone, which is a strict correlative of the boreal *W. tardus* Zone. This diachronous worldwide gap, along with the latest Smithian and earliest Spathian temperature and/or salinity changes (Romano et al., 2013; Goudemand et al., 2019) and the earlier (middle-late Smithian boundary) switch from wet to dry climate indicated by terrestrial plants (Hermann et al., 2011; Hochuli et al., 2016) are all pointing to a transition from a greenhouse to a more temperate or even cold climate during the late Smithian, with a modest extension into the basal Spathian. The middle Smithian recorded the most prominent negative CIE of the Early Triassic, coeval with changes in temperature and/or salinity (Romano et al., 2013), a major spore spike (Hermann et al., 2011) and Hg/TOC anomalies only known from the boreal record (Grasby et al., 2013; 2016). The earlier onset of the gap in the Boreal realm also supports early cooling at high latitude, thus choking the terrigenous flux towards marine shelves during the *G. sinuatum* Zone. In an equatorial SSB section from the South China block, a multiproxy geochemical analysis (Zhang et al., 2015) indicated reduced chemical weathering and sedimentation rates precisely at the SSB, at least locally. These proxies were interpreted as a cooling episode whose timing brings additional support for a diachronous onset of the cooling across latitude, spanning the entire latest Smithian *G. sinuatum* Zone. Moreover, the abrupt shape of the positive CIE documented by these authors conforms to that of most SSB shelf records in south China and in the northern Indian margin. This suggests again the presence of a gap intercalated between the *G. sinuatum* Zone and basal Spathian in the low latitudes. Hence, the late Smithian gap is apparently of global significance but started earlier in the Boreal records. On the other hand, the deep sea pelagic SSB record from the Panthalassic and near equatorial Mino Tamba Terrane highlights that both limbs and maximum of the positive CIE are all gradual (Sakuma et al., 2012). This argues against a substantial hiatus in sedimentation in the deep oceanic record. The age model constructed by these authors is based on the correlation of their deep sea $\delta^{13}C_{org}$ record with the well dated, but incomplete $\delta^{13}C_{carb}$ shelf records from South China. They inferred that sedimentation rate increased by an order of

magnitude during the late Smithian. However, they placed their middle-late Smithian boundary at the minimum of the negative CIE that is diagnostic of the middle Smithian. With the additional problem of large error bars on dates and correlations, the late Smithian cannot be distinguished from the middle Smithian in terms of sedimentation rate in this deep oceanic record. This rare deep sea $\delta^{13}C_{org}$ record nevertheless reveals that most of the interval with elevated sedimentation rate is in fact within the middle Smithian, in agreement with the shelf records from South China (e.g. Galfetti et al., 2007b).

Whatever the respective efficiency and share of potential CO_2 sinks that may contribute to the positive CIE (biological pump, buffering by marine carbonate - see Donnadieu et al. 2011; Jones et al., 2016), their cumulated effects may still be insufficient for bringing down the pCO_2 to the level where terrestrial ice can start forming at the poles. Temperature is also expected to closely track the carbon budget if feedback mechanisms are preponderant. However, in the northern Indian margin the delay of the temperature decrease (Goudemand et al., 2019) with respect to the earlier inception of the positive CIE and black shales deposition amounts to the duration of the early late Smithian *W. tardus* Zone. This delayed cooling suggests that some other primary mechanisms distinct from the feed back processes must have come into play. A decrease in global volcanism near the middle-late Smithian boundary is one potential explanation for this delay.

The Wallenbergfjellet section confirms that when preserved, the end of the positive CIE is of basal Spathian age and follows a gentle pot-bellied shape without abrupt jumps akin to that of deep sea records. The precise shape of the positive CIE is dictated by the distribution of gaps, sedimentation rates, and sample spacing. If the maximum of the CIE is erased by a gap, the correlation of any isotopic peak can be misleading in the absence of independent age control.

The mercury record from the Wallenbergfjellet section is worthy of particular attention, as it is the only current record across the SSB where TOC concentrations are regularly above 1 wt.%. This means that any changes in Hg/TOC ratios cannot be due to errors induced by low Hg or TOC concentrations.

The abrupt change from anomalously high Hg/TOC values in the Smithian to low levels in the Spathian (Figure 4) could be interpreted as a switch from elevated volcanism to little or background volcanic activity. However, this section differs from other published Hg/TOC anomalies of purported volcanic origin in that the elevated Hg/TOC values observed in the middle Smithian are moderate in magnitude, protracted (>18 m of section), and not accompanied by increased Hg concentrations (Figure 4). It is therefore important to consider alternative non-volcanic possibilities for changes in Hg/TOC concentrations.

Terrestrial and marine ecosystems are inherently different, leading to variations in nutrient cycling and thereby influencing the degree of Hg enrichments in various organic carbon reservoirs. Therefore, changes to the dominant source of organic matter could result in variations in Hg/TOC values, creating false Hg/TOC 'anomalies'. At present, potential differences in Hg/TOC values between terrestrial and marine sources are poorly understood, as there is a huge range of ecosystems in each realm that each have differing Hg-uptake pathways. There is some limited evidence to suggest that terrestrially derived sediments have higher background Hg/TOC values than fully marine sediments (Percival et al., 2015; 2017). This is corroborated with an apparent correlation of Hg/TOC anomalies with distance to shore from studies of the latest Triassic and early Toarcian, although it is unclear whether this represents higher Hg/TOC values in organic matter or another source such as clay minerals (Them II et al., 2019).

In this study, the increase in hydrogen index at the SSB in our data set could be caused by decreased oxidation and bioturbation, or by a shift to a dominance of marine organic matter. With the latter interpretation, the close correlation with Hg/TOC anomalies and terrestrially-sourced organic matter could be a cause for part or perhaps all of the step change in Hg/TOC values observed across the SSB in our data set (Figure 5B). The smaller Hg/TOC anomalies observed in this study compared to those observed at Festningen (Grasby et al., 2016) may support the hypothesis of Them II et al. (2019) that the magnitude of Hg/TOC anomalies are often positively correlated with proximity to paleoshoreline,

although the relatively high TOC concentrations throughout the section would suggest this is due to higher Hg/TOC values of terrestrially derived organic matter rather than adsorption onto clay surfaces.

Redox conditions are also critical to the dominant mode of Hg deposition (Them II et al., 2019), as a recent study from the Ordovician/Silurian boundary showed that Hg concentrations are governed by the prevalence of pyrite rather than organic matter under euxinic conditions (Shen et al., 2019b). The close correlation between Hg and Fe in the Wallenbergfjellet section (Figure 4; 5D) might suggest that Hg may indeed be partially associated with pyrite instead of organic matter. However, the clear change in hydrogen index between the Smithian and the Spathian (Figure 5B) could be a result of decreased oxidization of organic matter, thus suggesting the Spathian is the more anoxic environment. Moreover, Fe is ubiquitous in the Smithian Lusitaniadalen Member with minor occurrences of pyrite, while Fe is largely restricted to common framboidal pyrite in the Spathian Vendomdalen Member (Figure 6). If Hg was dominantly deposited by sulfides, then one would expect Hg/TOC ratios to be elevated in more anoxic strata, the opposite of what is observed across the SSB. Based on the data available, it therefore appears that sulfide deposition is not a controlling factor in variations to Hg/TOC anomalies when comparing Smithian and Spathian strata. However, there is clearly a correlation between Hg and Fe within the Spathian.

The scale and prolonged nature of the Hg/TOC anomalies in the middle Smithian are indicative of two mutually inclusive possibilities: 1) that terrestrial ecosystems in the Early Triassic have inherently higher Hg/TOC ratios than marine ecosystems; and/or 2) there was a sustained global Hg-enrichment that disproportionately affected the terrestrial realm. The magnitude of this protracted anomaly would suggest that elevated global volcanism, possibly from renewed activity from the Siberian Traps, is a plausible explanation. What is less clear is whether the low Hg/TOC concentrations observed in the early Spathian are due to a cessation of environmental Hg-enrichment, a change in organic matter source with Hg-enrichments limited to the terrestrial realm, or a combination thereof.

Unfortunately, there is little information on organic matter type at previously reported localities with Hg/TOC anomalies near the SSB (Arctic Canada and western Spitsbergen). There is also a substantial temporal offset (i.e. the *W. tardus* Zone) between the peak in Hg/TOC anomalies and the climax of the marine extinction at the SSB, challenging the hypothesis that volcanic degassing is the cause of the environmental crises at the SSB.

6. Conclusions

Middle -not late- Smithian times witnessed a thermal maximum as suggested by oxygen isotopic composition, rates of chemical weathering, biogeography of conodonts and the presence of a spore spike. Nektonic organisms responded to these adverse conditions by producing many short-lived species, as exemplified by the northern Indian margin ammonoid record (Brühwiler et al., 2010, Bucher et al. 2013). The extinction of the ammonoids and conodonts clearly post dates the middle Smithian thermal maximum and is intimately associated with a global gap at or close to the SSB and a late Smithian cooler and dryer climate. The Early Triassic Hg/TOC anomaly previously documented in Spitsbergen is here shown to be of middle Smithian age (*E. romunderi* Zone), thus questioning the role of volcanism as a trigger for the late Smithian extinctions and the commonly associated “lethally” hot scenario. A slight decrease in the Hg/TOC values is seen already in the late Smithian *W. tardus* Zone, coeval with or slightly predating the positive carbon isotope excursion marking the Smithian/Spathian boundary. Hg/TOC values then remain low through the Spathian.

The cause of this Smithian Hg/TOC anomaly is not fully resolved. Errors induced by low Hg or TOC values that affect other SSB localities can be discounted for this section due to sufficiently high (>0.5 wt.%) TOC concentrations. Redox proxies suggest less oxygenated conditions coinciding with low Hg/TOC ratios in the Spathian, which indicates that Hg deposition by sulfides is not a controlling factor in the difference between Smithian and Spathian strata. Crucially at Wallenbergfjellet, the termination of the elevated Hg/TOC values coincides with a shift in the hydrogen index, which can be

interpreted as a change from predominantly terrestrial to marine organic matter (although a decrease in oxidation is an alternative explanation). This suggests that it is possible that a change in the supply of organic matter from more terrestrial to more marine source may account for the observed differences in Hg/TOC values from the Smithian to the Spathian. This could be due to more efficient Hg-uptake in terrestrial ecosystems than marine environments at this time, and/or that there was an elevated Hg source to the environment, such as volcanism, that preferentially impacted the terrestrial realm. The former scenario does not require elevated volcanism from the Siberian Traps or elsewhere to account for the observed Hg/TOC record at Wallenbergfjellet, highlighting the need for caution when interpreting Hg/TOC anomalies in the Early Triassic (and potentially other time periods) as a signal of volcanism.

Acknowledgments

We are grateful to Franz-Josef Lindemann for invaluable help with the field work. The Swiss SNF (project 200020-160055) supported field and lab work of HB and ESH. MTJ is supported by the Research Council of Norway through its Centers of Excellence funding scheme, project number 223272, and the Research Council of Norway Unge Forskertalenter project 'Ashlantic', project number 263000. Stephen Crowley, Liverpool University, carried out the isotope analyses. Eirini Zacharaki, Natural History Museum, Oslo, assisted with SEM-EDX imaging. Tamsin Mather and Lawrence Percival are thanked for their help and assistance. We are highly grateful for constructive comments by Jun Shen, Thomas Algeo, and an anonymous reviewer.

References

Baresel, B., Bucher, H., Brosse, M., Cordey, F., Guodun, K. and Schaltegger, U. 2017. Precise age for the Permian–Triassic boundary in South China from high precision U-Pb geochronology and Bayesian age–depth modeling. *Solid Earth* 8, 361–378.

Baud, A., Magaritz, M., Holser, W.T., 1989. Permian-Triassic of the Tethys: Carbon isotope studies. *Geologische Rundschau* 78, 649–677.

Black, B.A., Elkins-Tanton, L.T., Rowe,M.C., Peate, I.U., 2012. Magnitude and consequences of volatile release from the Siberian Traps. *Earth and Planetary Science Lett*ers 317–318, 363–373.

Black, B.A., Lamarque, J.-F., Shields, C.A., Elkins-Tanton, L.T., Kiehl, J.T., 2014. Acid rain and ozone depletion from pulsed Siberian Traps magmatism. *Geology* 42, 67–70.

Bin, C., Xiaoru, W., Lee, F.S.C., 2001. Pyrolysis coupled with atomic absorption spectrometry for the determination of mercury in Chinese medicinal materials. *Analytica Chimica Acta* 447, 161–169.

Bower, J., Savage, K.S., Weinman, B., Barnett, M.O., Hamilton, W.P., Harper, W.F., 2008. Immobilization of mercury by pyrite (FeS_2). *Environmental Pollution* 156, 504–514.

Brayard, A., Bucher, H., Escarguel, G., Fluteau, F., Bourquin, S., Galfetti, T. 2006. The Early Triassic ammonoid recovery: Paleoclimatic significance of diversity gradients. *Palaeogeography, Palaeoclimatology, Palaeoecology* 239, 374–95.

Brayard, A., Bucher, H. 2008. Smithian (Early Triassic) ammonoid faunas from northwestern Guangxi (South China): Taxonomy and Biochronology. *Fossils and Strata 55*, 179 pp.

Brayard, A., Bucher, H. 2015. Permian-Triassic extinctions and rediversifications. In: C. Klug *et al*. (eds.), Ammonoid Paleobiology: From macroevolution to paleogeography. *Topics in Geobiology 44*, DOI 10.1007/978-94-017-9633-0_17.

Brayard, A., Escarguel, G., Bucher, H., Monnet, C., Brühwiler, T., Goudemand, N., Galfetti, T., Guex, J. 2009. Good genes and good luck: Ammonoid diversity and the end-Permian mass extinction. *Science* 325, 1118–1121.

Brühwiler, T., Bucher, H., Brayard, A., Goudemand, N. 2010. High-resolution biochronology and diversity dynamics of the Early Triassic ammonoid recovery: the Smithian faunas of the Northern Indian Margin. *Palaeogeography, Palaeoclimatology, Palaeoecology* 297, 491–501.

Bucher, H., Hochuli, P.A., Goudemand, N., Schneebeli-Hermann, E., Romano, C., Hautmann, M., Hofmann, R., Brayard, A., Vennemann, T., Weissert, H. 2013. Some like it hot: The Smithian diversification-extinction model. *GSA Abstracts with Programs* 45, 883.

Burgess, S.D., Bowring, S., Shen, S.-z., 2014. High-precision timeline for Earth's most severe extinction. *Proceedings of the National Academy of Science, USA* 111, 3316–3321. http://dx.doi.org/10.1073/pnas.1317692111.

Burgess, S.D., Bowring, S.A. 2015. High-precision geochronology confirms voluminous magmatism before, during, and after Earth's most severe extinction. *Science Advances* 1, e1500470.

Craig, H.S. 1957. Isotopic standards for carbon and oxygen and correction factors for mass-spectrometric analysis of carbon dioxide. *Geochemica et Cosmochimica Acta* 12, 133–149.

Dagys, A.S. 1994. Lower Triassic stage, substage and zonal scheme of north-eastern Asia. In: Guex, J., Baud, A. (eds) Recent developments on Triassic stratigraphy. *Mémoires de Geologie (Lausanne)* 22, 15–23.

Donnadieu, Y., Dromart, G., Goddéris, Y., Pucéat, E., Brigaud, B., Dera, G., Dumas, C., Olivier, N. 2011. A mechanism for brief glacial episodes in the Mesozoic greenhouse. *Paleoceanography* 26, PA3212.

Duan, Y., Han, D.S., Batchelor, B., Abdel-Wahab, A., 2016. Synthesis, characterization, and application of pyrite for removal of mercury. *Colloids and Surfaces A: Physicochemical and Engineering Aspects* 490, 326–335.

Durand, B., Monin, J.C. 1980. Elemental analysis of kerogens (C, H, O, N, S, Fe). Pp. 113-142, In Durand, B. (ed.): Kerogen – insoluble organic matter from sedimentary rocks. Éditions Technip, Paris.

Dypvik, H., Harris, N.B. 2001. Geochemical facies analysis of fine-grained siliciclastics using Th/U, Zr/Rb and (Zr+Rb)/Sr ratios. *Chemical Geology* 181, 131–146.

Ernst, R.E., Youbi, N. 2017. How large igneous provinces affect global climate, sometimes cause mass extinctions, and represent natural markers in the geological record. *Palaeogeography Palaeoclimatology, Palaeoecology* 478, 30–52.

Font, E., Adatte, T., Sial, A.N., Lacerda, L.D., Keller, G., Punekar, J., 2016. Mercury anomaly, Deccan volcanism, and the end-Cretaceous mass extinction. *Geology* 44, 171–174.

Frazer, J.W., Crawford, R. 1963. Modifications in the simultaneous determination of carbon, hydrogen, and nitrogen. *Mikrochimica Acta* 51, 561–566.

Galfetti, T., Hochuli, P.A., Brayard, A. Bucher, H., Weissert, H., Vigran, J.O. 2007a. Smithian-Spathian boundary event: Evidence for global climatic change in the wake of the end-Permian biotic crisis. *Geology* 35, 291-294. doi: 10.1130/G23117A

Galfetti, T., Bucher, H., Ovtcharova, M., Schaltegger, U., Brayard, A., Brühwiler T., Goudemand, N., Weissert H., Hochuli, P., Cordey, F., Guodon K. 2007b. Timing of the Early Triassic carbon cycle perturbations inferred from new U-Pb ages and ammonoid biochronozones. *Earth and Planetary Science Letters* 258, 593–604.

Golonka, J., 2011. Phanerozoic palaeoenvironment and palaeolithofacies maps of the Arctic region. In Spencer, A.M., Embry, A.F., Gautier, D.L., Stoupakova, A.V., Sørensen, K. (eds.), Arctic Petroleum Geology. *Geological Society, London, Memoirs*, 35, 79-129, doi: 10.1144/M35.6.

Goudemand, N., Orchard, M.J., Tafforeau, P., Urdy, S., Brühwiler, T., Brayard, A., Galfetti, T., Bucher, H. 2012. Early Triassic conodont clusters from South China: Revision of the architecture of the 15 element apparatuses of the superfamily Gondolelloidea. *Palaeontology* 55, 1021–1034.

Goudemand, N., Romano, C., Brayard, A., Hochuli, P.A., Bucher, H. 2013. Comment on "Lethally hot temperatures during the Early Triassic greenhouse". S*cience* 339 (6123), 1033.

Goudemand, N., Romano, C., Leu, M., Bucher, H., Trotter, J., Williams, I. 2019. Dynamic interplay between climate and marine biodiversity upheavals during the Early Triassic Smithian–Spathian biotic crisis. *Earth Science Reviews*, https://doi.org/10.1016/j.earscirev.2019.01.01

Grasby, S.E., Sanei, H., Beauchamp, B., Chen, Z. 2013. Mercury deposition through the Permo-Triassic biotic crisis. *Chemical Geology* 351, 209–216.

Grasby, S.E., Beauchamp, B., Bond, D.P.G., Wignall, P.B., Sanei, H. 2016. Mercury anomalies associated with three extinction events (Capitanian Crisis, Latest Permian Extinction and the Smithian/Spathian Extinction) in NW Pangea. *Geological Magazine* 153, 285–297.

Hammer, Ø., Harper, D.A.T., Ryan, P.D. 2001. PAST: Paleontological Statistics software package for education and data analysis. *Palaeontologia Electronica* 4(1), 9 pp.

Hardisty, D.S., Lyons, T.W., Riedinger, N., Isson, T.T., Owens, J.D., Aller, R.C., Rye, D.M., Planavsky, N.J., Reinhard, C.T., Gill, B.C., Masterson, A.L., Asael, D., Johnston, D.T. 2018. An evaluation of sedimentary molybdenum and iron as proxies for pore fluid paleoredox conditions. *American Journal of Science* 318, 527–556.

Hautmann, M. 2014. Diversification and diversity partitioning. *Paleobiology* 40, 162–176.

Hautmann, M., Bagherpour, B., Brosse, M., Frisk, Å., Hofmann, R., Baud, A., Nützel, Goudemand, N., Bucher, H. 2015. Competition in slow motion: The unusual case of benthic marine communities in the wake of the end-Permian mass extinction. *Palaeontology* 58, 871–901. doi: 10.1111/pala.12186

Hermann, E., Hochuli, P.A., Bucher, H., Brühwiler, T., Hautmann, M., Ware, D., Roohi, G. 2011. Terrestrial ecosystems on North Gondwana in the aftermath of the end-Permian mass extinction. *Gondwana Research* 20, 630–637.

Hochuli, P.A., Sanson-Barrera, A., Schneebeli-Hermann, E., Bucher, H. 2016. Severest crisis overlooked - Worst disruption of terrestrial environments postdates the Permian-Triassic mass extinction. *Nature Scientific Reports*. DOI: 10.1038/srep28372

Hubred, J.H. 2006. Thermal effects of basaltic sill emplacement in source rocks on maturation and hydrocarbon generation. Cand. Scient. Thesis, University of Oslo. Permanent link: http://urn.nb.no/URN:NBN:no-12609.

Jattiot, R., Bucher, H., Brayard, A., Monnet, C., Jenks J.F., Hautmann, M. 2015. Revison of the genus *Anasibirites* Mojsisovics. 1896 (Ammonoidea): An iconic and cosmopolitan taxon of the late Smithian (Early Triassic) extinction. *Papers in Palaeontology*. DOI: 10.1002/spp2.1036.

Jattiot, R., Bucher, H., Brayard, A., Brosse, M., Jenks, J.F., Bylund, K.G. 2017. Smithian ammonoid faunas from northeastern Nevada: implications for Early Triassic biostratigraphy and correlation within the western USA basin. *Palaeontographica Abteilung A* 309, 1–89.

Jenks, J.F., Brayard, A. 2018. Smithian (Early Triassic) ammonoids from Crittenden Springs, Elko County, Nevada: taxonomy, biostratigraphy and biogeography. *New Mexico Museum of Natural History & Science Bulletin* 78, 175 pp.

Jones, M.T., Jerram, D.A., Svensen, H.H., Grove, C. 2016. The effects of large igneous provinces on the global carbon and sulphur cycles. *Palaeogeography Palaeoclimatology Palaeoecology* 441, 4–21.

Jones, M.T., Percival, L.M.E., Stokke, E.W., Frieling, J., Mather, T.A., Riber, L., Schubert, B.A., Schultz, B., Tegner, C., Planke, S., Svensen, H.H., 2019. Mercury anomalies across the Palaeocene-Eocene Thermal Maximum. *Climate of the Past* 15, 1-20, doi:10.5194/cp-15-1-2019.

Kamo, S.L., Czamanske, G.K., Amelin, Y., Fedorenko, V.A., Davis, D.W., Trofimov, V.R., 2003. Rapid eruption of Siberian flood-volcanic rocks and evidence for coincidence with the Permian-Triassic boundary and mass extinction at 251 Ma. *Earth and Planetary Science Letters* 214, 75–91, doi:10.1016/S0012-821X(03)00347-9.

Keller, G., Mateo, P., Punekar, J., Khozyem, H., Gertsch, B., Spangenberg, J., Bitchong, A., Adatte, T., 2018. Environmental changes during the cretaceous-Paleogene mass extinction and Paleocene-Eocene thermal maximum: Implications for the Anthropocene. *Gondwana Research* 56, 69–89, doi:10.1016/j.gr.2017.12.002.

Komatsu, T., Takashima, R., Shigeta, Y., Maekawa, T., Tran, H.D., Cong, T.D., Sakata, S., Dinh, H.D., Takahashi, O. 2016. Carbon isotopic excursions and detailed ammonoid and conodont biostratigraphies around Smithian–Spathian boundary in the Bac Thuy Formation, Vietnam. *Palaeogeography, Palaeoclimatology, Palaeoecology* 454, 65–74.

Leu, M., Bucher, H., Goudemand, N. 2018. Clade-dependent size response of conodonts to environmental changes during the late Smithian extinction. *Earth-Science Reviews*, https://doi.org/10.1016/j.earscirev.2018.11.003

Lucas, S.G. 2018. The GSSP method of chronostratigraphy: A critical review. *Frontiers in Earth Science*, https://doi.org/10.3389/feart.2018.00191

Magaritz, M., Bart, R., Baud, A., Holser, W.T., 1988. The carbon-isotope shift at the Permian/Triassic boundary in the southern Alps is gradual. *Nature* 331, 337–339.

Major, H., Haremo, P., Dallmann, W.K., Andresen, A., 2001. Geological Map of Svalbard 1:100,000 Sheet C9G Adventdalen (Norsk Polarinstitutt Temakart, www.npolar.no).

Meyer, K.M., Yu, M., Jost, A.B., Kelly, B.M., Payne, J.L., 2011. $\delta^{13}C$ evidence that high primary productivity delayed recovery from end-Permain mass extinction. *Earth and Planetary Science Letters* 302, 378–384.

Mørk, A., Knarud, R., Worsley, D. 1982. Depositional and diagenetic environments of the Triassic and Lower Jurassic succession of Svalbard. In: *Arctic Geology and Geophysics* (eds. A.F. Embry, H.R. Balkwill), pp. 371–398. Canadian Society of Petroleum Geologists Memoir 8.

Mørk, A., Elvebakk, G., Forsberg, A.W., Hounslow, M.W., Nakrem, H.A., Vigran, J.O., Weitschat, W. 1999. The type section of the Vikinghøgda Formation: a new Lower Triassic unit in central and eastern Svalbard. *Polar Research* 18, 51–82.

Orchard, M.J. 2007. Conodont diversity and evolution through the latest Permian and Early Triassic upheavals. *Palaeogeography, Palaeoclimatology, Palaeoecology* 252, 93–117.

Orchard, M.J., Zonneveld, J.-P. 2009. The Lower Triassic Sulphur Mountain Formation in the Wapiti Lake area: lithostratigraphy, conodont biostratigraphy, and a new biozonation for the lower Olenekian (Smithian). *Canadian Journal of Earth Sciences* 46, 757–790.

Outridge, P.M., Sanei, H., Stern, G.A., Hamilton, P.B., Goodarzi, F., 2007. Evidence for control of mercury accumulation rates in Canadian High Arctic lake sediments by variations of aquatic primary productivity. *Environmental Science & Technology* 41, 5259–5265.

Ovtcharova, M., Goudemand, N., Hammer, Ø., Guodun, K., Cordey, F., Galfetti , T., Schaltegger, U., Bucher, H. 2015. Developing a strategy for accurate definition of a geological boundary through radio-isotopic and biochronological dating: the Early–Middle Triassic boundary (South China). *Earth-Science Reviews* 146, 65–76.

Paton, M.T., Ivanov, A.V., Fiorentini, M.LK., McNaughton, N.J., Mudrovska, I., Reznitskii, L.Z., Demonterova, E.I. 2010. Late Permian and Early Triassic magmatic pulses in the Angara-Taseeva syncline, Southern Siberian Traps and their possible influence on the environment. *Russian Geology and Geophysics* 51, 1012–1020.

Payne, J.L., Lehrmann, D.J., Wei, J., Orchard, M.J., Schrag, D.P., Knoll, A.H., 2004. Large perturbations of the carbon cycle during recovery from the end-Permian extinction. *Science* 305, 506–509.

Percival, L.M.E., Witt, M., Mather, T., Hermoso, M., Jenkyns, H., Hesselbo, S., Al-Suwaidi, A., Storm, M., Xu, W., Ruhl, M., 2015. Globally enhanced mercury deposition during the end-Pliensbachian extinction and Toarcian OAE: A link to the Karoo-Ferrar Large Igneous Province. *Earth and Planetary Science Letters* 428, 267–280.

Percival, L.M.E., Ruhl, M., Hesselbo, S.P., Jenkyns, H.C., Mather, T.A., Whiteside, J.H., 2017. Mercury evidence for pulsed volcanism during the end-Triassic mass extinction. *Proceedings of the National Academy of Sciences* 114, 7929-7934, doi: 10.1073/pnas.1705378114.

Percival, L.M.E., Jenkyns, H.C., Mather, T.A., Dickson, A.J., Batenburg, S.J., Ruhl, M., Hesselbo, S.P., Barclay, R., Jarvis, I., Robinson, S.A., Woelders, L., 2018. Does large igneous province volcanism always perturb the mercury cycle? Comparing the records of Oceanic Anoxic Event 2 and the end-Cretaceous to other Mesozoic events. *American Journal of Science* 318, 799–860, doi:10.2475/08.2018.01.

Pyle, D.M., Mather, T.A., 2003. The importance of volcanic emissions for global atmospheric mercury cycle. *Atmospheric Environment* 37, 5115–5124.

Ravichandran, M., 2004. Interactions between mercury and dissolved organic matter—a review. *Chemosphere* 55, 319–331.

Romano, C., Goudemand, N., Vennemann, T.W., Ware, D., Schneebeli-Hermann, E., Hochuli, P.A., Brühwiler, T., Brinkmann, W., Bucher, H. 2013. Climate and biotic upheavals following the end-Permian mass extinction. *Nature Geoscience* 6, 57–60.

Ruiz, W.L.G., Tomiyasu, T., 2015. Distribution of mercury in sediments from Kagoshima Bay, Japan, and its relationship with physical and chemical factors. *Environmental Earth Sciences* 74, 1175–1188.

Sakuma, H., Tada, R., Ikeda, M., Kashiyama, Y., Ohkouchi, N., Ogawa, N.O., Watanabe, S., Tajika, E., Yamamoto, S., 2012. High-resolution lithostratigraphy and organic carbon isotope stratigraphy of the Lower Triassic pelagic sequence in central Japan. *Island Arc* 21, 79–100.

Sanei, H., Grasby, S., Beauchamp, B., 2012. Latest Permian mercury anomalies. *Geology* 40, 63–66.

Sanei, H., Outridge, P.M., Stern, G.A., MacDonald, R.W., 2014. Classification of mercury-labile organic matter relationships in lake sediments. *Chemical Geology* 373, 87–92.

Scheyer, T.M., Romano, C., Jenks, J., Bucher, H. 2014. Early Triassic marine biotic recovery: The predators' perspective. *PLoS One*, DOI: 10.1371/journal.pone.0088987.

Schovsbo, N.H., Nielsen, A.T., Harstad, A.O., Bruton. D.L. 2018. Stratigraphy and geochemical composition of the Cambrian Alum Shale Formation in the Porsgrunn core, Skien-Langesund district, southern Norway. *Bulletin of the Geological Society of Denmark* 66, 1–20.

Selin, N.E., 2009. Global biogeochemical cycling of mercury: a review. *Annual Review of Environment and Resources* 34, 43–63.

Sepkoski Jr., J.J., 1996. Patterns of Phanerozoic extinction: A perspective from global databases, in Walliser, O.H., ed., Global Events and Event Stratigraphy in the Phanerozoic: Berlin, Springer-Verlag, 35–51.

Sepkoski Jr., J.J., 2002. A compendium of fossil marine animal genera. *Bulletins of American Paleontology* 363, 1–560.

Shen, J., Algeo, T.J., Hu, Q., Zhang, N., Zhoul, L., Xia, W., Xie, S., Feng, Q. 2012. Negative C-isotope excursions at the Permian-Triassic boundary linked to volcanism. *Geology* 40, 963–966.

Shen, J., Algeo, T.J., Planavsky, N.J., Yu, J.X., Feng, Q.L., Song, H.J., Song, H.Y., Rowe, H., Zhou, L., Chen, J.B. 2019a. Mercury enrichments provide evidence of Early Triassic volcanism following the end-Permian mass extinction. *Earth-Science Reviews*, accepted.

Shen, J., Algeo, T.J., Chen, J.B., Planavsky, N.J., Feng, Q.L., Yu, J.X., Liu, J.L. 2019b. Mercury in marine Ordovician-Silurian boundary sections of South China is sulfide-hosted and non-volcanic in origin. *Earth and Planetary Science Letters* 511, 130–140.

Sial, A., Lacerda, L., Ferreira, V., Frei, R., Marquillas, R., Barbosa, J., Gaucher, C., Windmöller, C., Pereira, N., 2013. Mercury as a proxy for volcanic activity during extreme environmental turnover: The Cretaceous-Paleogene transition. *Palaeogeography Palaeoclimatology Palaeoecology* 387, 153–164.

Sofer, Z. 1980. Preparation of carbon dioxide for stable carbon isotope analysis of petroleum fractions. *Analytical Chemistry* 52, 1389–1391.

Song, H.Y., Tong, J., Algeo, T.J., Horacek, M., Qiu, H., Song, H.J., Tian, L., Chen, Z.-Q. 2013. Large vertical $\delta^{13}C_{DIC}$ gradients in Early Triassic seas of the South China craton: Implications for oceanographic changes related to Siberian Traps volcanism. *Global and Planetary Change* 105, 7–20.

Sun, Y., Joachimski, M.M., Wignall, P.B., Yan, C., Chen, Y., Jiang, H., Wang, L., Lai X., 2012. Lethally hot temperatures during the early Triassic greenhouse. *Science* 338, 366-370.

Svensen, H., Planke, S., Polozov, A.G., Schmidbauer, N., Corfu, F., Podladchikov, Y.Y., Jamtveit, B., 2009. Siberian gas venting and the end-Permian environmental crisis. *Earth and Planetary Science Letters* 277, 490–500.

Them II, T.R., Jagoe, C.H., Caruthers, A.H., Gill, B.C., Grasby, S.E., Gröcke, D.R., Yin, R., Owens, J.D., 2019. Terrestrial sources as the primary delivery mechanism of mercury to the oceans across the

Toarcian Oceanic Anoxic Event (Early Jurassic). *Earth and Planetary Science Letters* 507, 62–72, doi:10.1016/j.epsl.2018.11.029.

Thibodeau, A.M., Ritterbush, K., Yager, J.A., West, A.J., Ibarra, Y., Bottjer, D.J., Berelson, W.M., Bergquist, B.A., and Corsetti, F.A., 2016. Mercury anomalies and the timing of biotic recovery following the end-Triassic mass extinction. *Nature Communications* 7, 11147.

Tong, J.,. Zhang, S., Zuo, J., Xiong, X. 2007. Events during Early Triassic recovery from the end-Permian extinction. *Global and Planetary Change* 55, 66–80.

Torsvik, T.H., Cocks, L.R.M., 2017. Earth History and Palaeogeography. *Cambridge University Press*, 317 pp., ISBN: 978-1-107-10532-4.

Tozer, E.T. 1967. A standard for Triasssic time. *Geological Survey of Canada Bulletin* 156, 103 p.

Tozer, E.T. 1994. Canadian Triassic ammonoid faunas. *Geological Survey of Canada Bulletin* 467, 1–663.

Tribovillard, N., Algeo, T.J., Lyons, T., Riboulleau, A. 2006. Trace metals as paleoredox and paleoproductivity proxies: An update. *Chemical Geology* 232, 12–32.

Wang, X., Cawood, P.A., Zhao, H., Zhao, L., Grasby, S.E., Chen, Z.-Q., Zhang, L. 2019. Global mercury cycle during the end-Permian mass extinction and subsequent Early Triassic recovery. *Earth and Planetary Science Letters 513*, 144–155.

Wignall, P.B., Bond, D.P.G., Sun, Y., Grasby, S.E., Beauchamp, B., Joachimski, M.M., Blomeier, D.P.G. 2016. Ultra-shallow marine anoxia in an Early Triassic shallow-marine clastic ramp (Spitsbergen) and the suppression of benthic radiation. *Geological Magazine* 153, 316–331.

Xie, S., Pancost, R.D., Wang, Y., Yang, H., Wignall, P.B., Luo, G., Jia, C., Chen, L., 2010. Cyanobacterial blooms tied to volcanism during the 5 m.y. Permo–Triassic biotic crisis. *Geology* 38, 447–450.

Zhang, L., Zhao, L., Chen, Z.-Q., Algeo, T.J., Li, Y., Cao, L. 2015. Amelioration of marine environments at the Smithian-Spathian boundary, Early Triassic. *Biogeosciences* 12, 1597–1613.

Zhang, L., Orchard, M.J., Brayard, A., Algeo, T.J., Zhao, L., Chen, Z.-Q., Lyu, Z. 2019. The Smithian/Spathian boundary (late Early Triassic): A review of ammonoid, conodont, and carbon-isotopic criteria. *Earth-Science Reviews*, https://doi.org/10.1016/j.earscirev.2019.02.014